Range-gated active short-wave infrared imaging for rain penetration

Adam Willitsford,* **David Brown, Kevin Baldwin, Randall Hanna, and Lindsey Marinello**

Johns Hopkins University Applied Physics Laboratory, Laurel, Maryland, United States

Abstract. A fixed wavelength optical parametric amplifier laser was constructed to create nanosecond pulsed light at 1527 nm for eye-safe range gated active short-wave infrared (SWIR) imaging. The laser pulse is generated using a Nd:YAG operating at 1064 nm to pump a potassium titanyle arsenate crystal in a single-pass geometry, resulting in ≈85 mJ at up to 28 Hz at 1527 nm with a pulse duration of ∼8 ns. The SWIR imager can be gated in as short as a 70-ns window (active time) with time steps as small as 5 ns (e.g., 0 to 70 ns and 5 to 75 ns). This allows for significant weather penetration by reducing the contribution from back-scattered photons reaching the receiver from scattering along the path prior to the imaging target. In addition, by converting to 1527 from 1064 nm, the maximum permissible exposure limit for eye-safety is ≈4 orders of magnitude larger, allowing for higher fluences without risk of injury. NEXRAD weather data along the line-of-sight were utilized to facilitate atmospheric propagation modeling via MODTRAN to retrieve an estimate of the path transmittance during testing. The integrated system herein is shown to extend imaging ranges with improvement factors of ≈2.5–3.1× during periods of rain. An image of a water tower at a 10-km range was generated with visibilities between 3 and 4 km during testing. © *The Authors. Published by SPIE under a Creative Commons Attribution 4.0 Unported License. Distribution or reproduction of this work in whole or in part requires full attribution of the original publication, including its DOI.* [DOI: 10.1117/1.OE.60.1.013103]

1 Introduction

Range-gated active imaging has been used to improve contrast and extend the operational imaging range during inclement weather.[1] The advantages of range-gated imaging include weather penetration and scattering mitigation, as well as the ability to create three-dimensional images or range/depth maps of a scene.[2–4] The process involves sending out a narrow (nanosecond) pulse of light to illuminate a target and only integrating the signal for the brief period when the reflected ballistic photons are due back at the receiver aperture. This gating eliminates unwanted signal due to backscattering events along the path, and as a result, improves contrast at range. In addition to weather penetration, range-gated active imaging provides improved contrast during times of good weather as well as scene-dependent range information.

The approach taken herein is to utilize a flash imaging setup in which each camera frame is illuminated by a single laser pulse as opposed to an accumulation mode that integrates multiple laser pulses per frame. Christnacher et al. (2014)[5] performed a comparison of the two modalities and showed that flash mode has several advantages over an accumulation approach as the camera's integration time is short enough to allow operation during the night or day. The short exposure time reduces background (due to stray and ambient light) and reduces the effects of turbulence as the turbulence fields are frozen. The challenge of the flash imaging approach is the need for high pulse energies to create an image from a single laser pulse. Additional postprocessing methods can be employed to improve image quality generated from flash mode, such as

---

*Address all correspondence to Adam Willitsford, adam.willitsford@jhuapl.edu

frame averaging. As such, the frame averaging approach can be employed for slowly varying scenes that are amenable to time-averaging to reduce noise from atmospheric rain attenuation and laser speckle.

2 Active SWIR Imager Design and Implementation

2.1 Eye-Safe Operation

Significant efforts were made to produce an active short-wave infrared (SWIR) imaging system that is eye-safe to allow for imaging capability that could be fielded in nearly any scenario without major efforts to contain the laser transmittance path. A Quantel CFR 300 laser was modified to produce output at 1527 nm. A photo and diagram of the laser, as delivered, are shown in Fig. 1. The stock frequency doubling crystal was removed to provide access to the 1064-nm pump wavelength. An optical parametric amplifier (OPA) [potassium titanyle arsenate (KTA)] crystal was introduced by repurposing the frequency doubler's housing for the KTA crystal. The $\frac{1}{4}$-waveplate and beam expanding optics were reconfigured to optimize the non-linear generation inside the KTA crystal. Following the KTA crystal are the addition of two dichroic mirrors that were setup to reflect the residual 1064-nm pump and the 3.5-μm idler into a beam dump while allowing for the 1527-nm pulse to exit the laser housing. The reconfiguration for 1527-nm generation is shown in Fig. 2. Once the reconfiguration was complete, the KTA crystal orientation was optimized to maximize the laser output at 1527 nm via fine angle tuning of the crystal axis relative to the pump. The end result was a 1527-nm laser with 85 mJ/pulse with a pulse duration of $\approx$8 ns. The outgoing laser pulse was sent through a beam expander that reduced the beam divergence to 3 mrad while increasing the beam size to $\approx$2 cm. The beam divergence was measured in the lab over a path of $\sim$5 m by measuring the beam spot size. In addition, the 3-mrad divergence was confirmed during the field test in which the beam was found to fill the water tower (30-m diameter) at a 10-km range. Utilizing these parameters, the nominal ocular hazard distance is found to be 18 m using the ANSI Z136.1 standard.[6,7]
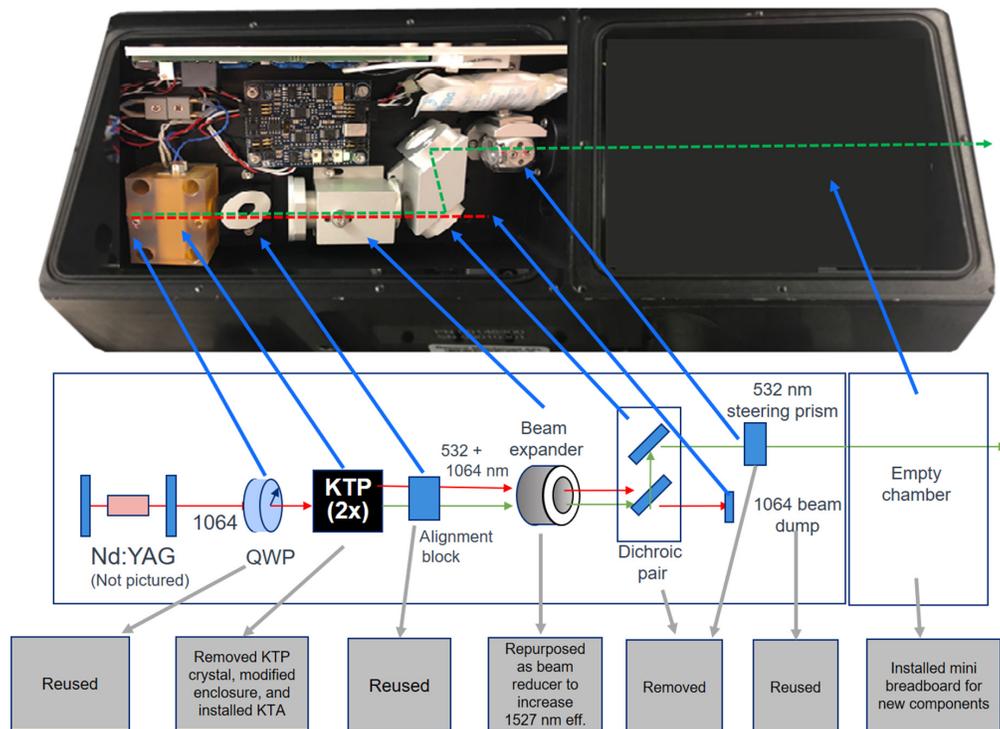
Fig. 1 Quantel CFR 300 as delivered. Many parts were repurposed and reused to maintain the laser operation within the original housing.
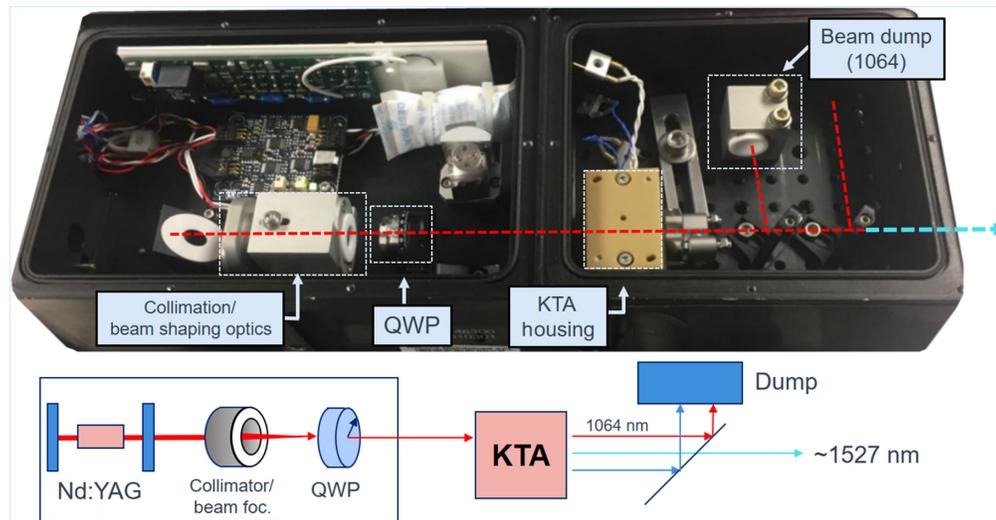
Fig. 2 Quantel CFR 300—postmodification for operation at 1527 nm—resulting in ≈85 mJ at up to 28 Hz.

2.2 Integrated System

The integrated laser transmitter and receiver are shown in Fig. 3. The Intevac LIVAR M506 camera (640 × 512-13.4 μm pixel pitch) was mounted to an Orion StarBlast F/4, 450-mm focal length Newtonian telescope. This resulted in a 30-μrad iFOV and a 0.98 deg × 0.86 deg field of view. The laser divergence of 3 mrad was chosen to maintain power density for long-range operation while filling a significant portion of the field of view. The laser and receiver were arranged in a monostatic configuration through the addition of an outgoing turning mirror glued behind the secondary of the imaging telescope, as shown in Fig. 3. This decision was made to ensure that the system retained boresight alignment for all propagation distances. To eliminate any range errors due to the laser's timing jitter, a high-speed photodiode was used as a master-sync to trigger the image acquisition for each laser pulse. The output of the photodiode response is used to trigger a Stanford Research Systems DG-535 that is utilized as the master delay clock, which then sends a transistor-transistor logic (TTL) pulse to trigger the camera's exposure. Utilizing this setup, the camera exposure is then delayed until the return of the pulse from the range of interest—in our case, ~10 km out and 10 km back from the water tower.

The integrated system was tested in clear conditions to confirm reliable operation. As a first test, a range/depth map of the water tower was constructed by sequentially delaying the
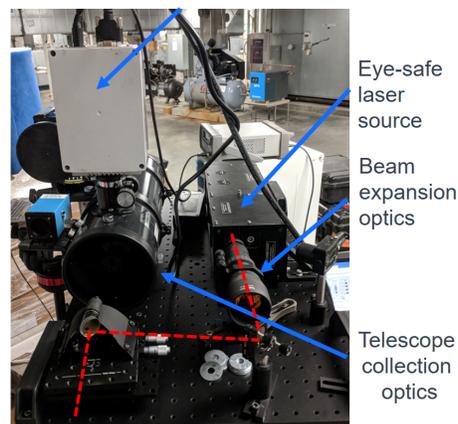
Fig. 3 SWIR active imaging integrated system. Laser path shown in red. The laser source was co-aligned with the collection optics, going out behind the secondary mirror of the imager.
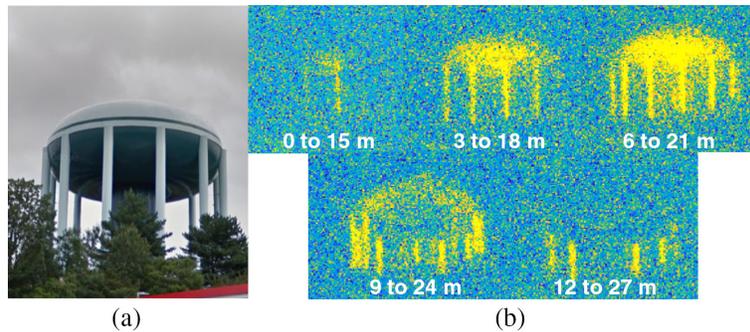
Fig. 4 (a) Water tower imaged locally from the ground ≈30 m in diameter. (b) Depth map of water tower as collected from the rooftop at JHU-APL at a 10-km range utilizing the range gated imager. The imager's exposure time was set to 100 ns and stepped by 20 ns to image the water tower from front to back. The 0- to 15-m exposure shows primarily the front support struts, whereas the 12- to 27-m exposure shows the rear supports.

range-gated imager's active exposure time over the laser pulse propagation. The SWIR imager was set with an exposure time of 100 ns corresponding to a 15-m exposure range and delayed in 20 ns (3 m) steps to effectively image different depths of the water tower. Figure 4(a) shows a visible image of the tower from close range. The water tower is ∼30 m in diameter with support struts evenly spaced around the base. Figure 4(b) shows the depth map created via the integrated range-gated SWIR imaging system from 10 km away. The application of incremental delays to the active time of the imager allowed for imaging of different range slices. The first range bin shows the front legs of the water tower. Subsequent increases in delays clearly reveal the side struts and the structure of the tower body. At the longest delay setting, the rear legs of the water tower are visible.

3 Active SWIR Imager Performance

A key motivation for developing an active imaging system is improved image quality at long range in spite of weather conditions that obscure the line-of-sight. In this section, results of a system-level test of the active SWIR imaging system are presented, followed by a detailed analysis of the performance. A key result is the gain in relative imaging range enabled by the active system. The relative range improvement factor is determined to be between 2.5 and 3.1.

During the system-level test, a water tower was actively imaged from a distance of 10 km. In Sec. 3.1, an overview of the integrated imaging system is provided. Test conditions and collected images are also reported. Section 3.2 presents an analysis of the atmospheric conditions at the time of testing, yielding an estimated rain rate and path transmittance along the line-of-sight to the water tower. In Sec. 3.3, image data from the test are analyzed to determine the normalized contrast of the range-gated active imager. The gain in imaging range is computed in this section, informed by the atmospheric characteristics reported in Sec. 3.2.

3.1 *Imagery Collection*

The range-gated active imager was operated in August 2019 from a rooftop on JHU/APL's campus, in Laurel, Maryland, to a water tower 10 km north–northeast. Figure 5 shows a satellite image of the 10-km path from APL's campus to the water tower, including a close-up view inset; the water tower is 30 m in diameter. A test of the range-gated imagers weather penetration capability was performed during a rainstorm during which visibility to the tower was lost. Figure 6(a) shows a passive visible image and passive SWIR image [Fig. 6(b)] of the line-of-sight from the rooftop to the water tower during the time of the test. Although obscured by rain, the water tower is centered in the field of view of both images.

For rain penetration, a 500-ns exposure time was used, yielding a 75-m range bin—this exposure was delayed by the out and back time to the water tower of 67.2 ms (10,080 m each way). A time series of flash illuminated (1 pulse/frame) frames operating at 20 Hz during a period of rain was collected and was postprocessed utilizing a 10-frame sliding window time average.
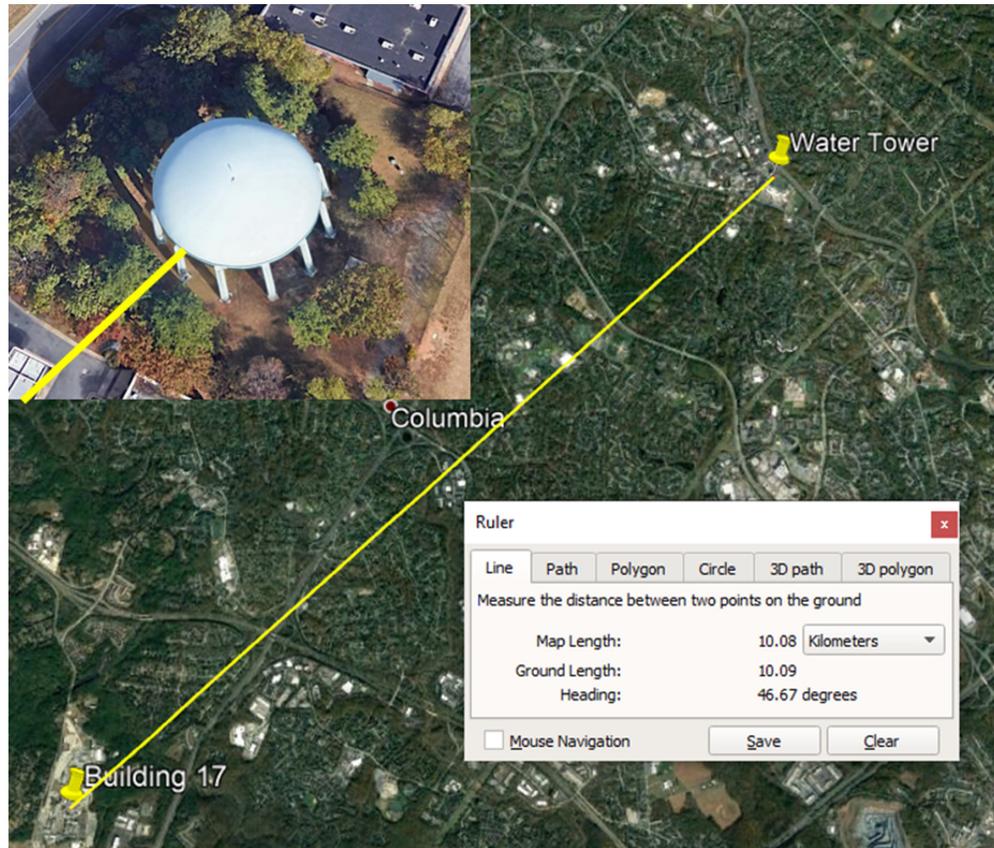
Fig. 5 Satellite image of the 10-km path from JHU/APL's facility to the water tower. Inset: zoomed image of the water tower with the line-of-sight marked in yellow. The water tower has a diameter of 30 m.

(a)   (b)
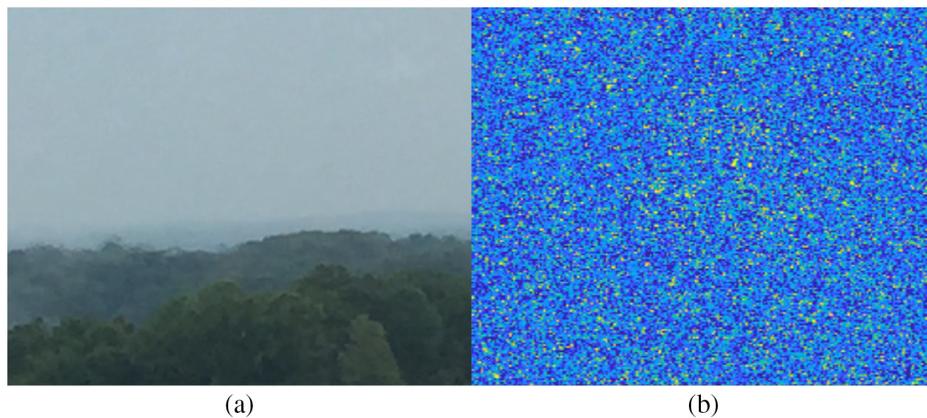
Fig. 6 (a) Passive visible camera image and (b) passive SWIR camera image during time of test.

A single-image frame can be seen in Fig. 7(a), and a typical 10-frame (0.5 s) sliding window average is shown in Fig. 7(b). Most notable is the significant increase in contrast as nearly the entire water tower becomes visible from the mitigation of rain effects and laser speckle.

3.2 Atmospheric Attenuation and Path Transmittance via MODTRAN

In this section, the atmospheric conditions at the time of the test were analyzed to estimate the line-of-sight transmittance during the test. Ultimately, these characteristics allow for a
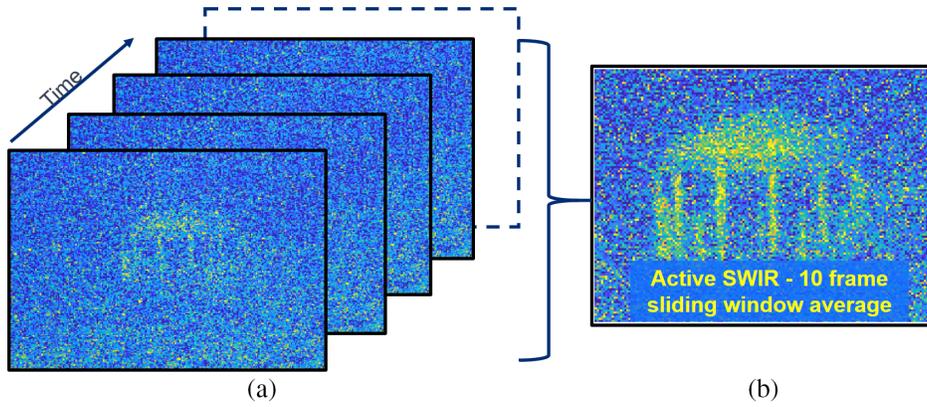
Fig. 7 Active SWIR images during the rain penetration test. (a) A single frame (500-ns exposure) and (b) a typical 10-frame sliding window average.

quantification of performance gains enabled by active imaging, which is discussed in Sec. 3.3. First, the path-averaged rain rate was determined using NEXRAD data from Sterling, VA. This rain rate was subsequently used to generate one-way 10-km path transmittance from the range-gated imager to the water tower as a function of wavelength for different visibility levels. The NEXRAD derived rain rate was processed to yield a path averaged rain rate over the 10-km path to the water tower. Figure 8(a) shows the NEXRAD derived rain rate with the optical
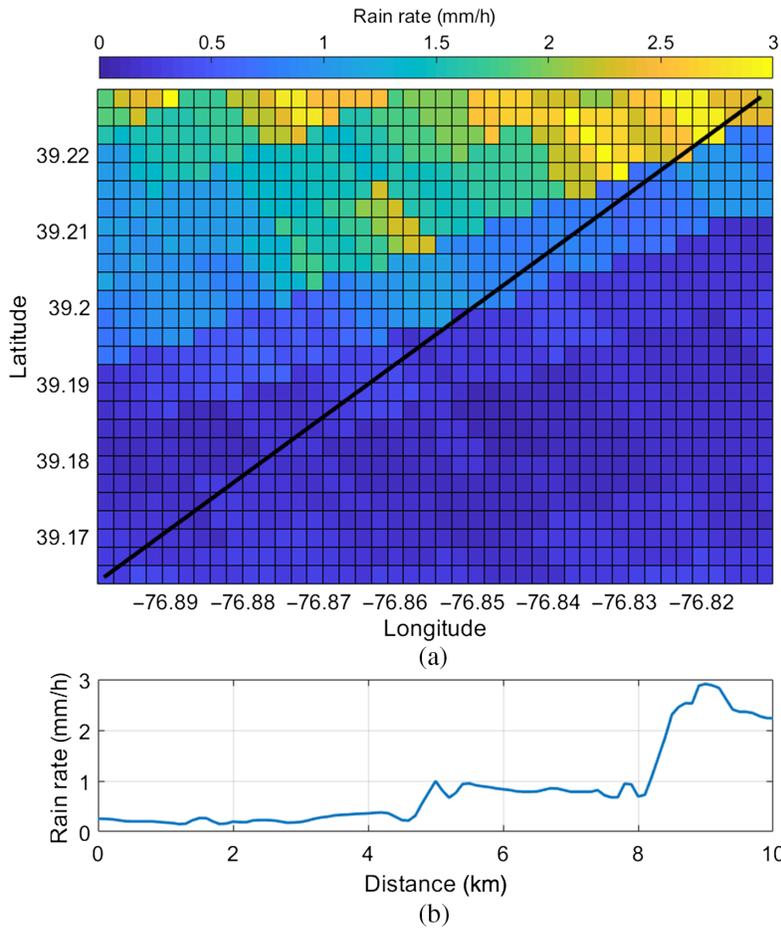
Fig. 8 (a) NEXRAD derived rain rate (mm/h) during the time of the test. The bold black line is the LoS from the transmitter to the water tower. (b) Rain rate (mm/h) along the line-of-sight. A path weighted average rain rate of 0.83 mm/h was calculated and used to seed Modtran.
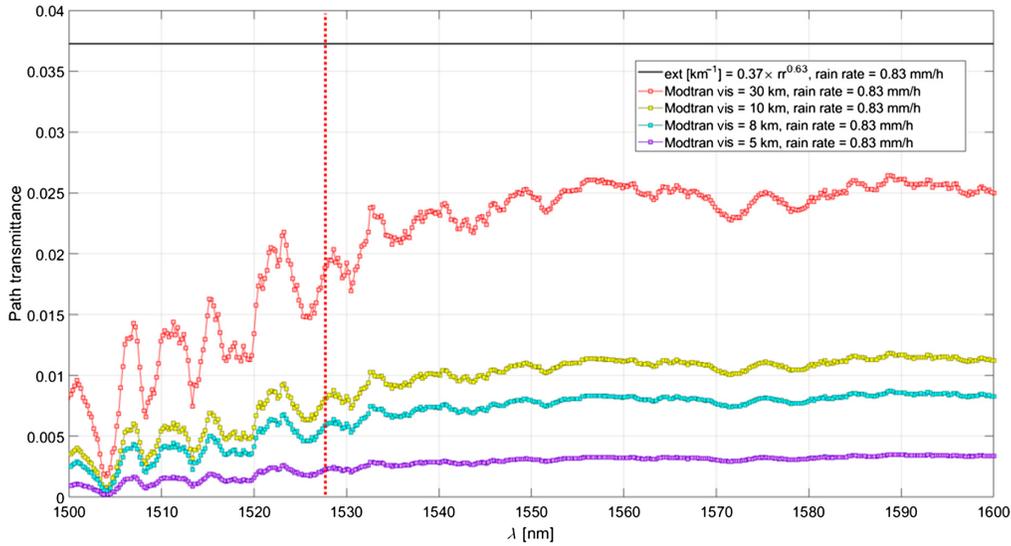
Fig. 9 One-way 10-km path transmittance from the laser source to the water tower. Top black curve is the transmittance solely due to the rain at 0.83 mm/h. The four color curves are the results of MODTRAN with the rain rate fixed and different visibilities. The dashed-red vertical line is the operational laser wavelength.

line-of-sight, overlaid in black. Figure 8(b) shows the rain rate as a function of distance along this line-of-sight. A path averaged rain rate of 0.83 mm/h was calculated at the time of test.

The path averaged rain rate was used to produce a one-way 10-km path transmittance from MODTRAN. MODTRAN is the moderate resolution transmittance model originally developed by the Air Force Research Lab (AFRL) to determine path transmittance and radiance for optical propagation.[8] A mid-latitude summer MODTRAN model was seeded using the path averaged rain rate of 0.83 mm/h along with an associated visibility that weights the aerosol loss along the path. The calculated transmittance curve, for the 10-km path to the water tower, as a function of wavelength is shown in Fig. 9.

The path transmittance, assuming no aerosol loss, was calculated by determining the extinction due to rain:[9,10]

$$\sigma(\text{km}^{-1}) = 0.37 \times [\text{rainrate}(\text{mm/h})]^{0.63}, \tag{1}$$

which yields an extinction value of 0.329 km^{-1} for a path averaged rain rate of 0.83 mm/h and a 10-km transmittance of 0.037. The rain rate driven extinction is, in general, independent of wavelength and is plotted in Fig. 9(a) as the black line. The MODTRAN model included both the effects of rain as an input as well as the aerosol extinction component, via the visibility input field. The resultant color curves show the variability in horizontal path transmittance over the 10-km path, with the rain rate set to 0.83 mm/h with different visibilities. It was abundantly clear that, since the water tower was not visible during testing, the visibility was <10 km and most likely around 5 to 8 km. Thus the teal and purple curves bound the transmittance as a function of wavelength, resulting in a one-way transmittance of 0.0025 to 0.006 at 1527 nm. The utilization of visibility as the aerosol loading factor within MODTRAN can be somewhat confusing, especially when also dealing with rain driven transmittance losses. Traditionally defined, visibility is a measure of all weather phenomena wrapped into a single observation. In this case, it is imperative to utilize both the rain rate and visibility to get an accurate representation of atmospheric transmittance. We calculate the extinction from the transmittance for the 10-km path via the following equation:

$$\sigma_{\text{ext}} = \frac{-\ln(\text{transmittance})}{\text{pathlength}}. \tag{2}$$

As a specific example, we will analyze the teal curve with a path averaged extinction at 1527 nm of $\sigma_{\text{ext}} = \ln(0.006)/10$ km $= 0.512/$km. The derived path extinction at 1527 nm

is used with the calculated contrast of the range-gated imager to determine the relative range improvement.

3.3 *Relative Range Improvement*

In the previous section, performance analysis was driven by atmospheric data. In this section, the image data were also processed to determine the contrast ratio and relative gain established by active imaging. In combination with the path extinction derived in the previous section, we utilize the normalized contrast metric to determine an equivalent visibility range for the system. This allows for a direct measure of range improvement enabled by active imaging, following an approach simliar to Christnacher et al.[11] To calculate the true range improvement, we need to determine the normalized contrast, e.g., the range-gated contrast in bad weather scaled to the clear day maximum contrast for the same time period. This was determined by imaging the water tower on a clear afternoon [Fig. 10(a) with optimal lighting conditions, and the contrast was found to be ≈0.22. The range-gated contrast during the rainstorm of the water tower was calculated for the images shown in Figs. 10(b) and (c). The mean of the pixel values for the background are calculated from the red box, and the signal is calculated for the black box on the water tower. Figure 10(b) shows a single frame from the range-gated imager (single laser pulse), Fig. 10(c) shows a 10-frame average (10 laser pulses). The contrast is calculated as follows:

$$C = \frac{\bar{S} - \bar{B}}{\bar{S} + \bar{B}}, \tag{3}$$

where $\bar{S}$ is the mean of the signal and $\bar{B}$ is the mean of the background. For the single frame, the contrast is 0.032, and for the 10 frame average, the contrast is 0.035. The active system is capable of maintaining a contrast of 3.2% at a range of 10 km. The 10-frame average shows a very
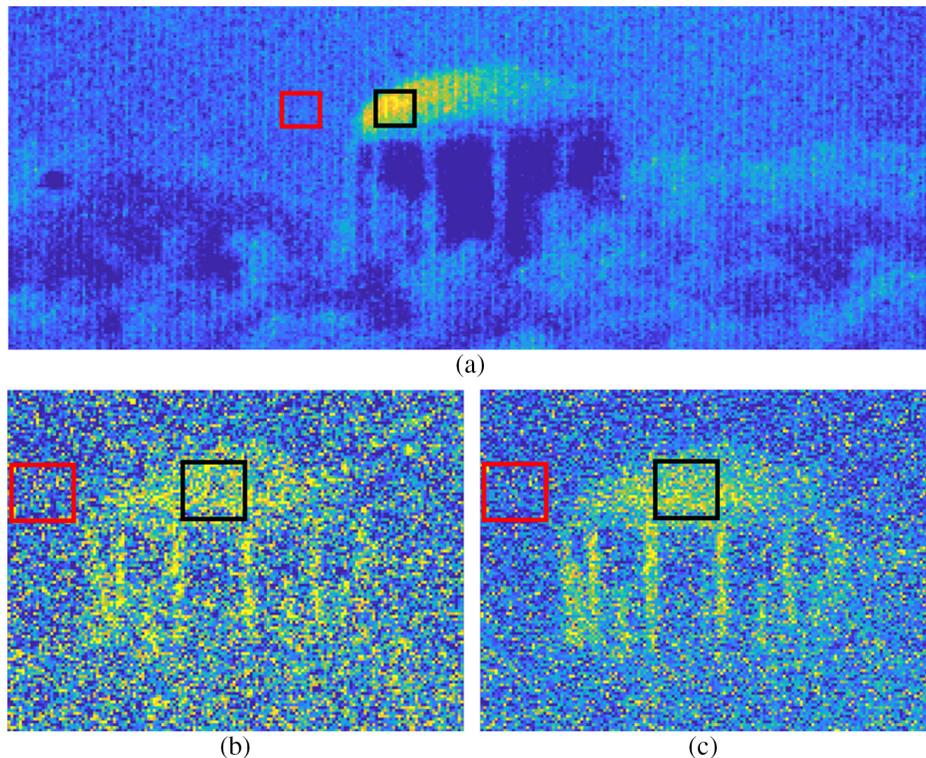
Fig. 10 (a) Clear day image of water tower used to calculate contrast for normalization metric; (b) single frame from range gated imager through rain; and (c) 10-frame average from range gated imager. Black boxes represent the regions where the background and signal were determined for the contrast calculation. The red box was used for the background and the black box on the tower was utilized for the signal.

marginal improvement over the single frame for the contrast determination. However, in terms of image recognition and edge determination, the 10-frame average shows distinct advantages by reducing laser speckle similar to results seen by Driggers et al.[12]

The normalized contrast from the imager ($0.032/0.22 = 0.145$) is used to calculate an equivalent path visibility to determine the relative range improvement factor. The equivalent visibility was determined for three transmittance values at 1527 nm, determined from Modtran in Fig. 9 utilizing Eq. (4) and summarized in Table 1. Given the most probable atmospheric extinction of 0.512 km^{-1} from Modtran atmospheric analysis, we see a range improvement factor of ~ 2.6. Table 1 shows that the range of our improvement factor is between 2.5 and 3.1, given the results of Modtran modeling:

$$\text{equivalent visibility} = \frac{-\ln(\text{normalized contrast})}{\sigma_{\text{ext}}}. \qquad (4)$$

We can similarly plot the normalized contrast as a function of attenuation lengths ($\sigma_{\text{ext}} \times$ range) and compare with the Beer–Lambert law. The Beer–Lambert law describes the constrast of a passive imager system as a function of attenuation lengths. Figure 11 shows the

Table 1 Contrast and relative range improvement for range gated imager in rain. The transmittance to extinction calculation is performed via Eq. (2) and the contrast to equivalent visibility is calculated via Eq. (4).

Transmittance → σ_{ext} (km^{-1})	Contrast → equivalent visibility (km)	Range improvement factor
0.008 → 0.483	0.145 → 4.0	$10/4.0 \approx 2.5$
0.006 → 0.512	0.145 → 3.8	$10/3.8 \approx 2.6$
0.0025 → 0.599	0.145 → 3.2	$10/3.2 \approx 3.1$
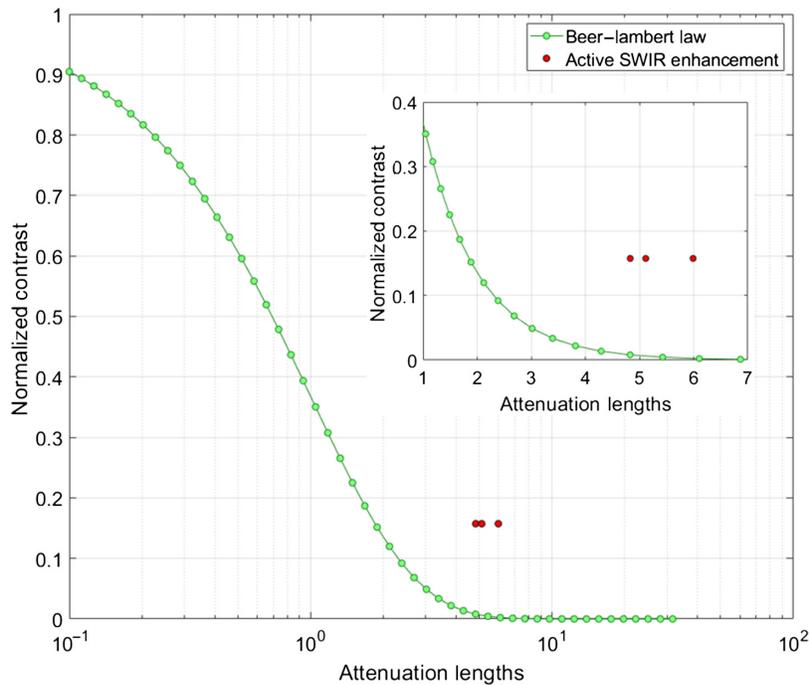
Fig. 11 Normalized contrast as a function of attenuation lengths for Beer–Lambert law evaluated at $\lambda = 1527$ nm and calculated normalized contrast of the range-gated imager. Normalized contrast of the imager was found to be 0.145 and is plotted for a 10-km range for each of the extinction values in Table 1. Inset: linear scale (attenuation length $= \sigma_{\text{ext}} \times$ range).

Beer–Lambert law normalized contrast as a function of attenuation lengths in green. The data from our test are shown as red dots. Looking at the plot, one can see that a normalized contrast of 0.145 should only be achievable at ∼2 attenuation lengths, whereas our active range gated system is capable of the same contrast at ≈5 to 6 attenuation lengths. Taking the ratio of the Beer–Lambert law attenuation lengths at a normalized contrast of 0.145 to the three plotted points (0.145 contrast at 4.8, 5.1, and 5.99 atten. lengths) results in the same values shown in Table 1 as the range improvement factor.

4 Conclusion

A fixed wavelength OPA laser for operation at 1527 nm (≈85 mJ up to 28 Hz) was constructed by retrofitting a commercial Quantel Nd:YAG laser with a KTA crystal designed for single-pass operation. The eye-safe laser was utilized as a pulsed illumination source for a range-gated flash (single pulse/frame) imaging system. The range-gated active SWIR imaging system has been shown to allow imaging beyond the conventional visibility limit. Using NEXRAD rain-rate information along the path line-of-sight in conjunction with atmospheric transmittance modeling via MODTRAN a fielded system was shown to enable imaging with improvement factors of ≈2.5 to 3.1× during periods of rain. The system was capable of imaging a target at the 10-km range with equivalent visibilities in the 3- to 4-km range. In addition, utilizing the high-speed gating capability, it was demonstrated that the system can produce an image plane depth map of the scene for regions that are not shadowed.

Acknowledgments

References

1. B. Gohler and P. Lutzmann, "Review on short-wavelength infrared laser gated-viewing at fraunhofer iosb," *Opt. Eng.* **56**(3), 031203 (2017).
2. P. Andersson, "Long-range three-dimensional imaging using range-gated laser radar images," *Opt. Eng.* **45**, 034301 (2006).
3. M. Laurenzis, F. Christnacher, and D. Monnin, "Long-range three-dimensional active imaging with superresolution depth mapping," *Opt. Lett.* **32**(21), 3146–3148 (2007).
4. R. Tobin et al., "Three-dimensional single-photon imaging through obscurants," *Opt. Express* **27**(4) (2019).
5. F. Christnacher, M. Laurenzis, and S. Schertzer, "Theoretical and experimental comparison of flash and accumulation mode in range-gated active imaging," *Opt. Eng.* **53**, 043106 (2014).
6. A. Augustoni, "Approximation methods for estimating the eye-safe viewing distances, with or without atmospheric transmission factors considered, for aided and unaided viewing conditions," Sand Report—Sand2002-1315, Sandia National Laboratories (2002).
7. ANSI, "Ansi z136.1—safe use of lasers," Laser Safety Report, The Laser Institute (2020).
8. A. Berk et al., *Modtran Manual 5.4.0 User's Manual*, The ONTAR Corporation (2016).
9. B. Miers, "Review of calculations of extinction for visible and infrared wavelengths in rain," Final Report DTIC—Accession Number: AD. A132659, Atmospheric Sciences Lab (1983).
10. C. Ulbrich and D. Atlast, "Extinction of visible and infrared radiation in rain: comparison of theory and experiment," *J. Atmos. Ocean. Technol.* **2**, 331–339 (1985).
11. F. Christnacher et al., "Influence of gating and of the gate shape on the penetration capacity of range-gated active imaging in scattering environments," *Opt. Express* **23**, 32897–32908 (2015).
12. R. Driggers et al., "Impact of speckle on laser range-gated shortwave infrared imaging system target identification performance," *Opt. Eng.* **42**, 738–746 (2003).

Adam Willitsford recieved his BS degree in electrical and computer engineering from Layafette College in 2002 and his PhD in electrical engineering from Pennsylvania State University in 2008. He is a member of the senior professional staff in the Optics and Photonics Group at Johns Hopkins University Applied Physics Laboratory. In addition, he teaches the fundamentals of lasers in the engineering for professionals program at Johns Hopkins University. His research interests include active and passive remote sensing and imaging systems as well as statistical analysis of EO/IR atmospheric propagation.

David Brown received his BS and MS degrees and his PhD in electrical engineering from Pennsylvania State University in 2003, 2005, and 2008, respectively. He is a member of the principal professional staff in the Optics and Photonics Group at Johns Hopkins University Applied Physics Laboratory. In addition, he teaches laser systems and applications in the engineering for professionals program at Johns Hopkins University. His research interests include high-energy laser systems and propagation, optical sensing, and numerical simulation.

Kevin Baldwin received his BS and MS degrees in optics from the University of Rochester in 1990 and 1991, respectively, his MS degree in electrical engineering from Rochester Institute of Technology in 1993, and his MSE degree and PhD in electrical engineering from Johns Hopkins University in 1995 and 1998, respectively. He is a member of the principal professional staff at Johns Hopkins University Applied Physics Laboratory and is chief engineer of the Engineering and Test Group within the Force Projection Sector. His research interests include active and passive imaging systems for long-range terrestrial, marine, and underwater applications.

Randall Hanna received his BS degree in physics from Ohio State University in 2015 and his MS degree in applied physics and his MS degree in data science from Johns Hopkins University in 2018 and 2021, respectively. He is a member of the associate professional staff in the Optics and Photonics Group at Johns Hopkins University Applied Physics Laboratory. His interests include passive and active imaging systems, as well as propagation through inhomogeneous media.

Lindsey Marinello received her BA degree in physics and Russian from Bryn Mawr College in 2017. She is a photonics engineer in the Optics and Photonics Group at Johns Hopkins Applied Physics Laboratory within the Air and Missile Defense Sector. She is also an MSc student part-time in the Department of Applied and Computational Mathematics (anticipated 2021) at Johns Hopkins University. Her research interests span topics from spacecraft dynamics and control to optical/photonic systems.